

INTERACTION OF LASER RADIATION WITH MATTER. LASER PLASMA https://doi.org/10.1070/QEL16377

Laser-induced microplasma as a tool for microstructuring transparent media*

V.P. Veiko, S.A. Volkov, R.A. Zakoldaev, M.M. Sergeev,
A.A. Samokhvalov, G.K. Kostyuk, K.A. Milyaev

Abstract. **We have studied the properties of laser-induced microplasma (LIMP) emerging in the ablation of a strongly light-absorbing target in the regime of confinement of spatial plasma expansion. The LIMP particle temperature is shown to be higher in this case than in the free expansion. It is found that the amplitude of the pressure pulse in the regime of spatial LIMP confinement is an order of magnitude higher than in the open surface case. The feasibility of writing microstructures on transparent dielectrics with the use of LIMP is demonstrated: microlens arrays and different diffraction elements are made.**

Keywords: *laser plasma, ablation, graphite, transparent dielectric, microstructuring.*

1. Introduction

In this work the term 'laser-induced microplasma' (LIMP) is used in reference to laser erosion plasma produced at the interface of transparent and absorbing media in the ablation of the latter. The special LIPM existence conditions consist in the regime of LIMP expansion confinement, when a transparent medium is a condensed medium, a liquid or a solid, rather than the air. When the gap width between the transparent and absorbing media is comparable with the roughness of the surfaces, there emerges a special plasma, which is characterised by special parameters and requires special methods of investigation. The keen interest in this microplasma arises from the possibility of controlling its localisation and physical parameters, which permits the wide use of LIMP for microstructuring the surface of transparent dielectrics. The action of LIMP produced in the ablation of an absorbing medium underlies several techniques for processing transparent dielectrics, beginning with the pioneering application – laser drilling in diamond dies [1] – and ending with laser-induced plasma-assisted ablation (LIPAA), laser-induced backside dry etching (LIBDE), laser-induced frontside etching (LIFE), etc. [2–8]. The medium transparent to the laser radiation may either be at complete contact with an absorbing medium [1, 4, 5, 8] or be some distance away from it [5–7]. In this case the gap width, the laser parameters being equal, has a significant effect on the LIMP properties and the configuration of the microstructures obtained on the surface of the transparent medium

We emphasise that the LIMP properties in the regime of expansion confinement are strongly different from the freely expanding plasma properties. For instance, it is well known that the glow intensity of the ion component of laser-produced plasma is much higher in the presence of a limiting medium [9, 10]. Another significant effect is an increase in the pulse amplitude of the pressure on the target (the effect of laser peening) [11], etc. However, the works on the LIMP structuring of transparent dielectrics [1–8] are primarily technology-oriented and present no measurements and analysis of the physical mechanism or specificity of the application of LIMP as a new technological instrument for the microprocessing of transparent media. That is why the investigation of LIMP properties in the regime of spatial expansion confinement is a topical task from the fundamental point of view as well from the standpoint of understanding the potentialities of LIMP optimisation and further application.

The objective of our work is to study the properties of the LIMP produced in complete contact of a transparent dielectric with a target exhibiting a strong absorption of laser radiation as well as to demonstrate the capabilities of the proposed version of the technique, namely laser-induced black body ablation (LIBBA), for the processing of transparent dielectrics.

2. Efficiency analysis of LIMP as a tool for microprocessing transparent dielectrics

When we address a generalised LIMP scheme (Fig. 1), it becomes clear that the optimal use of LIMP, as applied to the formulated problem, calls for its possession of the following parameters.

1. A high temperature [$(0.5–1)\times10^4$ °C] and a sufficiently high ion density, which is easiest to achieve for a nanosecond duration of laser pulses and their intensity sufficient for the optical breakdown at the target in the focusing to a spot 30–50 μm in size. Furthermore, the plasma should be a source of pulse periodic (not continuous, which is unacceptable for precision processing [12]), concentrated energy.

A comparison of the requisite parameters with the parameters of existing lasers as well as the executed experiments and general considerations about the efficiency and reliability of these lasers allow a conclusion that the optimal laser source for exciting the LIMP with the requisite parameters now is a

*Presented at the Fundamentals of Laser Assisted Micro- and Nanotechnologies (FLAMN-2016) International Symposium (Pushkin, Leningrad oblast, 27 June to 1 July 2016).

V.P. Veiko, S.A. Volkov, R.A. Zakoldaev, M.M. Sergeev, A.A. Samokhvalov, G.K. Kostyuk, K.A. Milyaev ITMO University, Kronverksky prosp. 49, 197101 St. Petersburg, Russia;
e-mail: vadim.veiko@mail.ru, samokhvalov.itmo@gmail.com

Received 24 March 2017
Kvantovaya Elektronika **47** (9) 842–848 (2017)
Translated by E.N. Ragozin

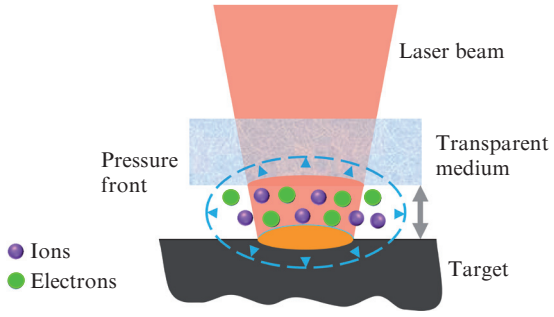

Figure 1. Generalised LIMP scheme.

pulsed ytterbium fibre laser, which has a high beam quality and a sufficiently high pulse energy.

2. A high laser beam energy to microplasma energy conversion efficiency, which calls for minimisation of the optical and thermal loss, requires a low light reflection coefficient from the target material and short exposures to laser radiation.

The combination of these requirements has led us to opt for graphite as a target material, which satisfies the above requirements for nanosecond exposures to the radiation of the fibre laser. Specifically, the reflection coefficient R of graphite at a wavelength of 1.06 μm amounts to 0.1–0.2 (for $T < 7000$ K) [13], while the thermal loss, which may be estimated from the ratio between the heated and evaporated volumes, does not exceed 5% under our conditions, although it depends heavily on the laser spot size.

Therefore, the energy efficiency of the LIMP induced by the fibre laser radiation is practically close to 100% as applied to a graphite target. And when the efficiency of using LIMP for processing transparent media is compared with the efficiency of their direct laser processing, the advantage of LIMP becomes evident.

The efficiency of the LIMP action also depends significantly on the gap between the transparent and absorbing media. When the gap is initially absent, the efficiency is much higher than even with a small (several tens of micrometres) gap, which is supposedly due to critical changes in LIMP properties at the interface in the occurrence of the gap.

3. A small (micro)plasma plume with controllable section size and position in space. As for the position of the plume at the media interface, it is evidently determined by the position of the laser beam and is strictly attached to it, while the transverse section of the hot plasma core is defined by the focal spot size and the gap width. Hence there follows the third fundamental feature of LIMP as a microprocessing tool: the requirement of complete contact between the transparent medium and the absorbing target, a so-called confinement regime.

The above requirements all are inherent in the LIMP configuration proposed by the authors, which received the name laser-induced black body ablation (LIBBA).

3. Setup and conditions of the experiment

In the experiment schematised in Fig.2a use was made of a pulsed fibre laser (*1*) (IPG-Photonics) with an output wavelength of 1.06 μm, a pulse energy of up to 1 mJ for a pulse duration $\tau = 200$ ns, and a pulse repetition rate of 1.6–100 kHz. The radiation of the laser source was focused with a flat-field objective lens (*2*) to a ~50 μm diameter spot on the surface of a graphite target (*3*). The role of the medium confinfing the LIMP expansion was played by fused silica (*4*), whose plate was tightly pressed to the graphite plate. The LIMP emission spectra were investigated using an LIBS2500-5 Ocean Optics spectrometer (*5*) with a spectral range of 395–890 nm, a spectral resolution of 0.1 nm, and a fibre input. The pickup fibre made an angle of ~70° to the target surface. The spectra were recorded with the aid of a personal computer (PC) (*6*), which also controlled the laser.

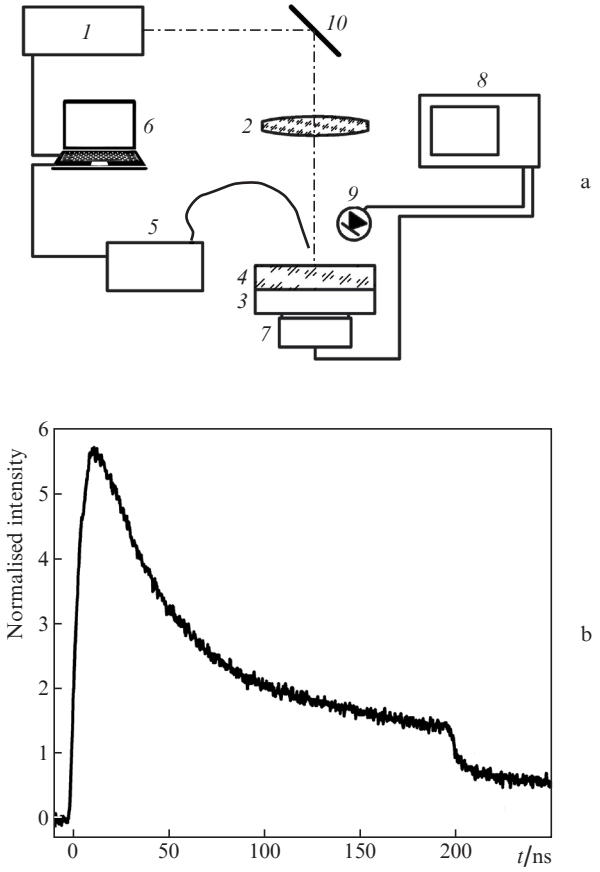

Figure 2. (a) Schematic of the experimental setup [(*1*) pulsed fibre laser; (*2*) focusing objective lens; (*3*) graphite target; (*4*) transparent dielectric; (*5*) fibre spectrometer; (*6*) PC; (*7*) ultrasonic sensor (US); (*8*) oscilloscope; (*9*) pin photodiode; (*10*) scanning device] and (b) the oscilloscope trace of a laser pulse used in our experiments.

In the recording of emission spectra, the laser pulse repetition rate was equal to 20 kHz. In this case, the target was rotated by an electric motor with a linear velocity of 5 m s^{-1} to rule out the reablation of the same area of the graphite target during the spectrometer exposure time (10 ms). In the investigation of acoustic LIPM parameters, we used a listhium niobate-based sensor (*7*) with a bandwidth of ~30 MHz for a 50 Ω load. The sensor was attached to the rear surface of the graphite target and the acoustic contact was provided by vacuum grease. The laser source was operated in a single-pulse regime. The photoacoustic signals were recorded with a Tektronix TDS3052C oscilloscope (*8*). A pin photodiode (*9*) monitored the arrival of the optical pulse.

To produce microstructures by changing the surface relief of fused silica, use was made of a GSI Lumonics G325DT scanning system (*10*), which consisted of two mirrors with

galvanic driver mechanisms. The scanning program was imposed by the PC. The external appearance of the resultant microstructures was investigated using a Carl Zeiss optical microscope in the transmitted and reflected light. The microrelief depth and the surface roughness were measured with a Hommel Tester T8000 contact profilometre. Separate craters were studied with an NT-MDT atomic force microscope.

4. Experimental results

Figure 3 shows the LIMP emission spectra recorded in the ablation of a graphite target in the case of free LIMP expansion and in the regime of its expansion confinement.

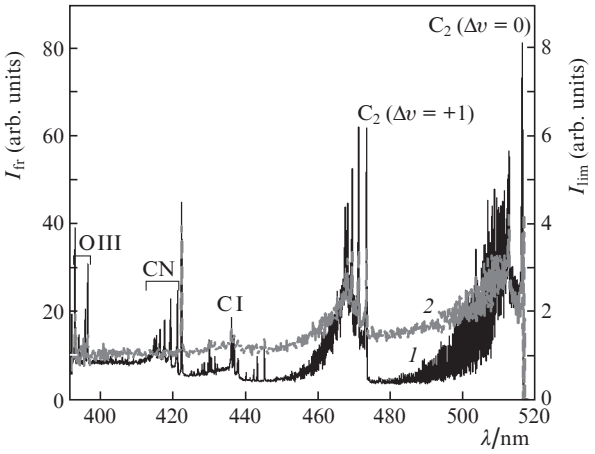

Figure 3. Typical LIMP emission spectra in the ablation of graphite in the case of (*1*) free LIMP expansion and (*2*) in the confinement regime. The laser intensity is equal to 70 MW cm^{-2}.

In the ablation of the graphite target under a fused silica plate, the intensity of LIMP emission spectra turned out to be an order of magnitude lower than in the free plasma expansion. Apart from the system of Swan bands, in the resultant LIMP spectra we identified the line of excited carbon atom CI (λ = 437.13 nm) and some lines of oxygen ions OIII (393.15 nm), OII (396.62 nm). The dependences of the glow intensity of different particles on the laser intensity I_{las} are depicted in Fig. 4 for both cases of graphite target ablation. One can see that the dependences of the LIMP glow on I_{las} in the ablation in the air and under the fused silica plate are different.

A significant feature of the spectrum emitted in the case of LIMP confinement is the existence of a strong continuum, which we attribute to the radiation of the graphite target as a black body, with the line spectrum imposed on it. We note that the possibility of significant substance overheating in the case of its expansion confinement in the laser irradiation was investigated in Refs [14, 15], which showed that this technique may be validly used to investigate the phase diagrams of the substance up to critical parameters.

We estimated the plasma temperature from the experimental emission spectra of C_2 molecules recorded in the regime of LIMP expansion confinement as well as in the free expansion. To estimate the vibrational plasma temperature T_{vib}, we measured the emission intensities of the Δv = +1 sequence bands in the electronic–vibrational–rotational

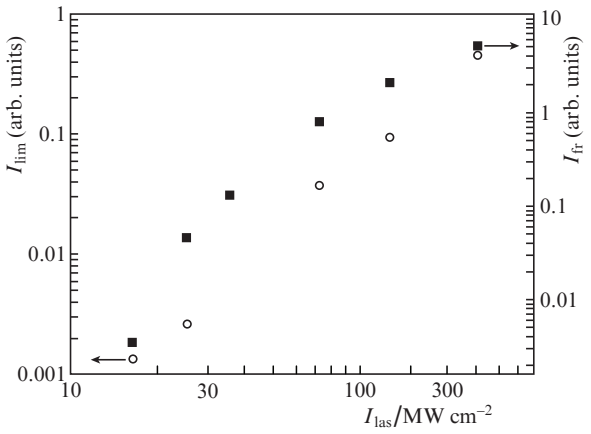

Figure 4. Dependences of the glow intensity of C_2 radicals (Δv = 0, λ = 516.4 nm) on the laser intensity in the case of LIMP expansion confinement by fused silica (circles) and in the free expansion of the plasma plume (squares).

spectrum of the Swan system of the C_2 molecule. We used a formula relating the band intensities to the value of the vibrational temperature:

$$\ln \frac{I_{v'v''}}{v^4_{v'v''} q_{v'v''}} = -\frac{G(v')}{kT_{vib}} + C, \qquad (1)$$

where $G(v')$ is the vibrational energy; $I_{v'v''}$ is the intensity of emission from vibrational level v'; $q_{v'v''}$ is the Frank–Condon factor for this transition; $v_{v'v''}$ is the radiation frequency; and k is the Boltzmann constant. Formula (1) is known and obtained by taking the logarithm of the classical formula for the emission intensity of one rotational line [16] with account taken of the Boltzmann population distribution of vibrational and rotational levels with the corresponding temperatures T_{vib} and T_{rot} (the latter circumstance is an assumption made in our work). The vibrational temperatures were determined from the slope of the characteristic straight lines drawn by the least squares method through the experimental points corresponding to spatially confined LIMP and the LIMP in the free expansion (Fig. 5). One can see that $T_{vib} \sim$ 14400 K in the regime of spatially confined LIMP, which is

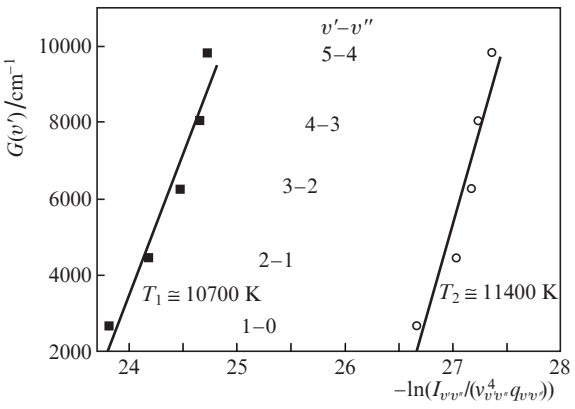

Figure 5. Dependences of $-\ln[I_{v'}/(v^4_{v'v''}q_{v'v''})]$ on the vibrational energy $G(v')$ of carbon LIMP in its free (squares) and confined (circles) expansion.

much higher than the temperature T_{vib} in the free expansion ($\sim$10700 K).

To estimate the rotational plasma temperature, we modelled the emission spectrum of the $\Delta v = +1$ sequence in the electronic–vibrational–rotational spectrum of the Swan system of the C_2 molecule. The simulation spectrum was compared with the experimental one, the rotational and vibrational plasma temperatures being the fit parameters in this case. The simulation spectrum was formed by summing the emission intensities of the rotational lines in every electronic-vibrational $\Delta v = +1$ sequence band (with consideration of the overlapping of band tails) by the formula

$$I_{j'j''}(\lambda) = \sum_{v'=1}^{8} \sum_{j'j''} \varepsilon_{j'j''}(v',\lambda) g(\lambda - \lambda_{j'j''}), \qquad (2)$$

where $\varepsilon_{j'j''}$ is the emission intensity of an individual rotational line and $g(\lambda - \lambda_{j'j''})$ is the form factor of the lines. The emission intensity of an individual rotational line was calculated by the classical formula, the Frank–Condon factors borrowed from Ref. [17] being used for the calculation. The rotational line strengths were calculated with the inclusion of λ splitting by formulas from Ref. [16]. The results of simulations are depicted in Fig. 6 along with the experimental spectrum. A comparison of the simulation and experimental spectra suggests that the calculated vibrational temperature agrees nicely with its value obtained by the method of relative intensities. The simulation values of the rotational and vibrational temperatures also do not contradict the results of Refs [18, 19].

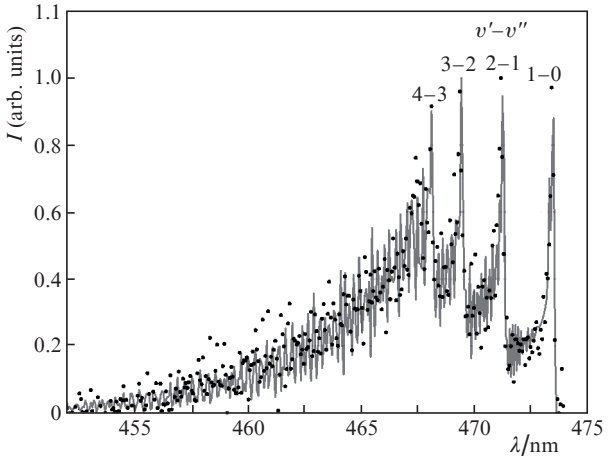

Figure 6. LIMP simulation emission spectrum of the C_2 molecule band under fused silica (points) and experimental data (solid curve) for a laser intensity of 70 MW cm^{-2} and $T_{vib} \sim 11500$ K, $T_{rot} \sim 4500$ K.

With the photoacoustic measurements we found that the behaviour of the photoacoustic signal as a function of the laser intensity in the ablation in the air was significantly different from its behaviour in the ablation under fused silica. In the former case, the photoacoustic signal linearly depends on the intensity, while in the latter case, it grows according to a close-to-power ($\sim I_{las}^{0.5}$) law and practically saturates at high intensities (Fig. 7). We also note that the photoacoustic signal is considerably (several times) higher in the ablation under fused silica than in the ablation in the air.

In the case of ablation in the LIMP expansion confinement regime, the pressure exerted by the laser-plasma-generated shock wave was estimated by the model of Ref. [11], in which the intensity dependence of the pressure is described by a power law: $P \sim I_{las}^{0.5}$. One can see from Fig. 7 that the experimental dependence is close to the model one and that the peak pressure amounts to $\sim$1 GPa.

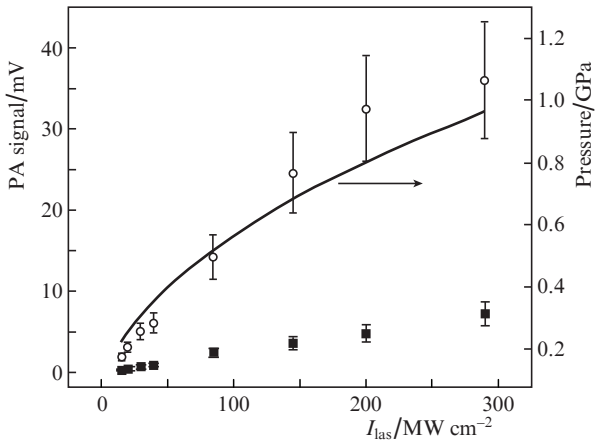

Figure 7. Dependences of the photoacoustic (PA) signal on the laser intensity for free (squares) and confined (circles) LIMP expansions. The solid curve shows the LIMP pressure dependence on the laser intensity in the expansion limitation mode calculated according to the model of Ref. [10].

Therefore, the properties of the LIMP under fused silica are significantly different from its properties in the free expansion. The effect of LIMP expansion confinement is responsible for an increase in the plasma pressure on the target, which in turn affects the ionic composition and thermodynamic parameters of the plasma: the density and temperature of the particles. The lowering of plasma glow intensity in the expansion confinement regime may be due to the change in the kinetics of the reactions occurring in the plasma because of the isochoricity of laser plume expansion. And it is likely that the lowering of glow intensity may be caused by energy redistribution between the ion and molecular LIMP components. Hence a conclusion may be drawn that the degree of LIMP ionisation in the case of expansion confinement is higher than in the free expansion.

5. Use of LIMP in its expansion confinement refime for structuring transparent dielectrics

The possibility of controlling the precision of a microrelief produced in the processing of glass by the LIMP technique is an important problem, whose solution called for a detailed study of the dependence of relief depth on the processing conditions. In particular, we determined experimentally the dependence of the resultant relief depth on the intensity of laser radiation. Figure 8 shows the profile of an isolated crater produced in fused silica under single-pulse irradiation; one can see the crater has an elevation approximately 100 nm in height.

Figure 8b shows the relief depth in the surface scanning at a velocity $v = 250$ mm s^{-1}, which provides the desired overlapping of the laser spots. One can see that it depends linearly on I_{las}.

By controllable laser beam scanning, with the help of an experimental facility (see Fig. 2) we obtained microlens arrays with lens diameters ranging from 80 to 300 μm, a sag of up to 1–2 μm, a radius of curvature down to 3 mm, a focal length

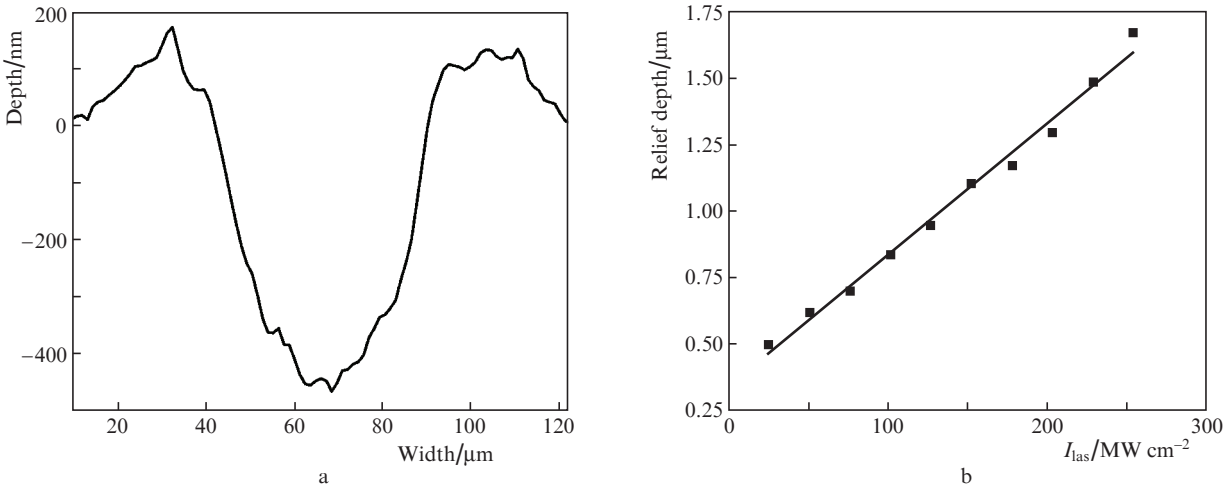

Figure 8. (a) Crater (the sectional view was obtained with an atomic-force microscope) in fused silica produced by exposure of a graphite target to a single laser pulse (I_{las} = 20 MW cm^{-2}, τ = 200 ns) and (b) depth of the relief produced by laser irradiation (v = 250 mm s^{-1}, ν = 20 kHz, t = 200 ns) as a function of I_{las}.

ranging from 5 to 10 mm (Figs 9a and 9b). The microlens arrays were tested in optical schemes of a nonimaging integrator and employed for the multibeam microprocessing of thin titanium films [5].

Laser beam scanning along a straight trajectory permitted writing phase diffraction gratings (PDGs) with rectangular and sinusoidal profiles (Figs 9c and 9d). The period of these PDGs varied in a range of 25–200 μm and could be smoothly varied, which was also provided by the scanning system. It was possible to vary the relief height in a range of 0.2–5.0 μm with increments of 60 ± 10 nm. The experimental PDG samples, which were predesigned for radiation wavelengths of 0.645 and 1.064 μm and then made by LIMP processing, were put to test in different optical configurations. In particular, we demonstrated the possibility of employing them as laser beam splitters. Depending on the regime of laser processing, it was possible to make PDGs capable of splitting a laser beam into three beams of equal intensity as well as into a larger number of beams whose intensities smoothly decreased as the order number receded from the zero order [4]. The dif-

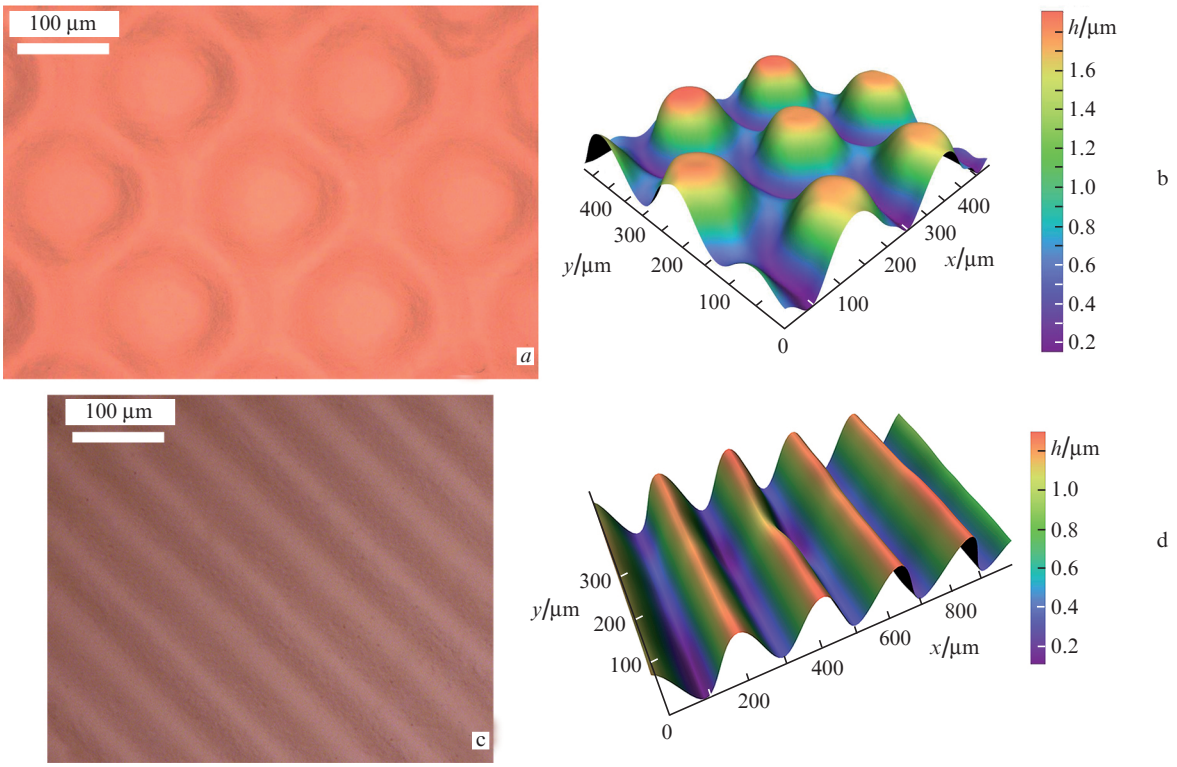

Figure 9. External appearance of (a) a microlens array and (b) its three-dimensional profile, as well as external appearance of (c) a phase diffraction grating and (d) its three-dimensional profile. The photos were taken in reflected light.

fraction elements of this type exhibit a low optical loss (below 10%) and may be employed in the optical schemes intended for multibeam microprocessing, for instance, of thin films.

Furthermore, the LIMP technique for the microprocessing of glass made it possible to write multilevel (up to five levels) diffraction elements of optical quality. This possibility was validly used to produce random phase plates of binary and discrete structure. The diffraction elements of this type were employed for homogenizing high-power laser beams [5]. The depth of the relief formed in these elements was varied between 0.15 and 5 μm and could be set with increments of 60 ± 10 nm for a phase element size of 250–350 μm.

We note that the efficiency (and controllability) of the processing of transparent dielectrics, for instance of fused silica, in the LIBBA configuration is, on the whole, comparable to the efficiency (and precision) of the ablation of metals with close thermophysical characteristics (for instance, of steel) for the same intensities of absorbed radiation and exposure durations. In experiments wherein there is a gap between the absorbing target and the dielectric [2], the processing depth achieved in one 7-ns long laser pulse amounts to several tens of nanometres. When there is a close contact in the LIBBA configuration, the ablation depth may be hundreds of times greater and may range up to several micrometres per pulse [5]. At the same time, the method permits making a relief several tens of nanometres in depth and thereby controlling its depth with an accuracy of 50 nm when the laser intensity is varied.

6. Discussion of the mechanism of transparent dielectrics structuring in the LIBBA configuration

In this Section we draw attention to the fact that the emission plasma spectrum contains both the lines of excited C_2 molecules, whose vibrational temperature amounts to ~14400 K, and the lines of carbon ions of considerably higher intensity. The ion component bombards the dielectric surface, which undoubtedly leads to its sputtering. At present, the ion sputtering mechanism is considered as the molecular analog of the macroscopic processes of mechanical bombardment: the formation of microcracks and the subsequent 'cluster' ablation (in contrast to evaporative – atomic ablation). The efficiency of this mechanism (the specific removal of substance) in the presence of excess pressure, which exceeds 1 GPa, is much higher than the efficiency of evaporation or two-phase thermal ablation [20].

Furthermore, the ions, unlike photons, transfer their energy almost completely to the lattice of any material, including a material transparent to optical radiation. At the same time, it is well to bear in mind that the laser-induced plasma contains ions with energies greater than the band gap of a dielectric, which results not only in its direct ablation, but also in a change of its optical properties. In particular, it gives rise to induced light absorption in the dielectric, which exists for more than several tens of microseconds [21] and may result in a more efficient absorption of the subsequent laser pulses.

Another significant aspect of microplasma action on a substance is the lifetime of carbon LIMP, which far exceeds the duration of a laser pulse [22]. In our experiments we used nanosecond laser pulses with a half-amplitude duration of ~50 ns and a ~150-ns long tail (see Fig. 2b). Under this ablation regime, the plasma is produced at the peak of the laser pulse or with some delay at its leading edge, depending on the intensity I_{las}. Therefore the energy in the tail of the laser pulse and the radiation of the long-lived carbon LIMP are efficiently absorbed in the resultant medium, which may explain the weak LIMP glow intensity in the expansion confinement regime.

7. Conclusions

The present work is concerned with the carbon LIMP investigated in expansion confinement regime with the use of optical emission spectroscopy. This regime was compared with the LIMP free expansion regime and it was shown that the former case exhibited a significantly higher LIMP pressure on the target and a lower intensity of the molecular component in the emission spectrum. In this connection, assumptions were made about the mechanism of transparent medium ablation in this regime, which is underlain by action of ions. We also noted the virtues of the LIMP technique in the processing transparent media, which comprise: (1) a high efficiency of using laser energy; 2) a high specific material removal efficiency, which is achieved due to the bombardment of the transparent medium by plasma ions and excess pressure in complete contact with the target; and 3) a high controllability of the microplasma owing to the strict relation of its position and size to those of the focused laser beam.

As a result, the proposed LIBBA configuration of the LIMP technique exhibits high precision and productivity, making it competitive with direct laser irradiation in the processing of transparent media. We demonstrated the technological capabilities of this 'laser-plasma tool' for microstructuring transparent dielectric surfaces and producing various microoptical elements like diffraction optical elements, microlens arrays, etc.

Acknowledgements. The reported study was financially supported by the Ministry of Education and Science of the Russian Federation, research agreement No. 14.587.21.0037 (RFMEFI58717X0037).

References

1. Veiko V.P., Libenson M.N. Inventor's certificate No. 300977. Priority of 05.09.1969. Registered in the Public Register of Inventions of the USSR on 22.01.1971.
2. Hanada Y., Sugioka K., Gomi Y., Yamaoka H., Otsuki O., Miyamoto I., Midorikawa K. *Appl. Phys. A*, **79**, 1001 (2004).
3. Lorenz P., Ehrhardt M., Zimmer K. *Phys. Procedia*, **39**, 542 (2012).
4. Blonskii I.V., Dan'ko A.Ya., Kadan V.N., Oreshko E.V., Puzikov V.M. *Zh. Tekh. Fiz.*, **75**, 74 (2005).
5. Kostyuk G.K., Sergeev M.M., Zakoldaev R.A., Yakovlev E.B. *Opt. Las. Eng.*, **68**, 16 (2015).
6. Chao H., Furong L., Min W., Jianwen Y., Jimin C. *J. Las. Applic.*, **24**, 022005 (2012).
7. Zhang J., Sugioka K., Midorikawa K. *Appl. Phys. A*, **67**, 545 (1998).
8. Hopp B., Smausz T., Vass C., Szabó G., Böhme R., Hirsch D., Zimmer K. *Appl. Phys. A*, **94**, 899 (2009).
9. Popov A.M., Colao F., Fantoni R. *J. Anal. At. Spectrom.*, **24**, 602 (2009).
10. Shen X.K., Sun J., Ling H., Lu Y.F. *Appl. Phys. Lett.*, **91**, 081501 (2007).
11. Fabbro R., Fournier J., Ballard P., Devaux D., Virmont J.J. *Appl. Phys.*, **68**, 2 (1990).
12. Metev S.M., Veiko V.P. *Laser-Assisted Microtechnology* (Springer, 1994).
13. Bulgakov A.V., Bulgakova N.M. *Quantum Electron.*, **29**, 433 (1999) [*Kvantovaya Elektron.*, **27**, 154 (1999)].

14. Karabutov A.A., Kubyshkin A.P., Panchenko V.Ya., Podymova N.B., Savateeva R.V. *Quantum Electron*., **28**, 670 (1998) [*Kvantovaya Elektron*., **25**, 690 (1998)].
15. Ivochkin A.Yu., Kaptilniy A.G., Karabutov A.A., Ksenofontov D.M. *Laser Phys*., **22**, 1220 (2012).
16. Ochkin V.N. *Spektroskopiya nizkotemperaturnoi plazmy* (Low-Temperature Plasma Spectroscopy) (Moscow: Fizmatlit, 2006).
17. Kuzyakov N.E., Kuz'menko L.A., Kuznetsova Yu.Ya. *Faktory Franka–Kondona dvukhatomnykh molekul* (The Franck–Condon Factors of Diatomic Molecules) (Moscow: Izd. MGU, 1984).
18. Dem'yanenko A.V., Letokhov V.S., Puretskii A.A., Ryabov E.A. *Quantum Electron*., **27**, 983 (1997) [*Kvantovaya Elektron*., **24**, 1012 (1997)].
19. Dem'yanenko A.V., Letokhov V.S., Puretskii A.A., Ryabov E.A. *Quantum Electron*., **28**, 33 (1998) [*Kvantovaya Elektron*., **25**, 36 (1998)].
20. Veiko V.P., Metev S.M., Kaidanov A.I., Libenson M.N., Jakovlev E.B. *J. Phys. D: Appl. Phys*., **13**, 1565 (1980).
21. Hanada Y., Sugioka K., Midorikawa K. *Proc. SPIE*, **6261**, 626111 (2006).
22. Harilal S.S., Hassanein A., Polek M. *Appl. Phys*., **110**, 053301 (2011).